Available online at www.sciencedirect.com
SCIENCE DIRECT®
International Journal of Thermal Sciences 42 (2003) 435–446
International Journal of Thermal Sciences
www.elsevier.com/locate/ijts

Experimental study on rising velocity of nitrogen bubbles in FC-72

P. Di Marco *, W. Grassi, G. Memoli

LOTHAR, Department of Energetics "L. Poggi", University of Pisa, via Diotisalvi 2, 56126 Pisa, Italy

Received 3 May 2002; accepted 11 July 2002

Abstract

In this work, the rising velocities of gas bubbles in a still liquid are measured and compared with available theories. In order to separate the mechanical effects from the thermal and mass exchange ones in bubble dynamics, adiabatic two-phase flow conditions were established by injecting gas (nitrogen) bubbles in a fluoroinert liquid (FC-72) at ambient temperature and pressure through an orifice (about 0.1 mm diameter) drilled on a generatrix of a horizontal tube. Bubble size, aspect ratio, detachment frequency, velocity and frequency of shape oscillations were measured by processing of high speed video images (at 1500 fps). A sensible steady oscillation of velocity, with a amplitude up to 20% of the mean value, was evidenced after the initial acceleration region. This oscillation was well correlated with the one in aspect ratio, thus providing evidence of the separate influence of this last parameter on drag coefficient. Available correlations did not give fully satisfactory results in predicting the mean rising velocity, showing a general tendency to underprediction. Sensible wake effects were excluded. Finally, the frequency of shape oscillation and the mean aspect ratio were compared with available models, evidencing their limitations.

Keywords: Bubble dynamics; Bubble rising velocity; Bubble drag coefficient

1. Introduction

1.1. State of the art

Several experimental and theoretical studies, on the motion of gas bubbles in a liquid have been performed since early 60s, and it is impossible to deal exhaustively with them all in this limited space. The problem was tackled, among the others, by Peebles and Garber [1], Davidson and Schuler [2,3], Kumar and coworkers [4–7], Wraith [8], Tsuge and Hibino [9], Zun and Groselj [10], Park et al. [11], Bhaga and Weber [12], Grace et al. [13], Pamperin and Rath [14], Buyevich and Webbon [15], Tomiyama [16], Tomiyama et al. [17]. Good reviews on the subject were compiled by Clift et al. [18], and Tsuge [19]. All of these studies are performed using two-component immiscible fluids (gas into liquid), in adiabatic conditions, and most of them were related to the motion of air bubbles in water or water-based mixtures. Only a few works were focused on different fluids (e.g., [9,11]) and, as far as known, none of them on organic refrigerants. Very recently Celata et al. [20,21] considered the motion of bubbles in a one-component system consisting of saturated FC-72, investigating the effect of pressure up to the critical one. The present work bridges the gap between the former ones on adiabatic systems and the work of Celata et al. on FC-72, in that for the first time rising velocity data are reported for an adiabatic system in which FC-72 is the operating fluid.

1.2. Dynamics of bubble motion

In this paper the vertical motion of a gas bubble in a still liquid is studied. The liquid is of different nature than the gas of the bubble. If evaporation of liquid and gas dissolution are neglected, the bubble has a constant mass, and furthermore, if the variation of temperature and pressure along its path are negligible, the volume of the bubble is constant too. Under these assumptions, the momentum equation along the vertical (y) axis can be written as

$$V_B \frac{\mathrm{d}}{\mathrm{d}t}\left[(\rho_g + C_M \rho_l) u_B\right] = (\rho_l - \rho_g) V_B g - F_D \tag{1}$$

where u_B is the velocity of the center of mass of the bubble. The contribution due to the inertia of the gas, represented by ρ_g on LHS of Eq. (1), is always neglected. If the trajectory of the bubble does not deviate significantly from the vertical,

* Corresponding author.
E-mail address: lothar@ing.unipi.it (P. Di Marco).

1290-0729/02/$ – see front matter
doi:10.1016/S1290-0729(02)00044-3

Nomenclature

A	area	m^2	
A_u	amplitude of velocity oscillation	m	
a	bubble minor axis	pixel	
a'	acceleration to buoyancy ratio		
b	bubble major axis	pixel	
c	bubble size in motion direction	m	
C_D	drag coefficient		
C_M	virtual mass coefficient		
d_{eq}	bubble equivalent diameter, Eq. (4)	m	
E	bubble aspect ratio		
$\overline{E}$	bubble mean aspect ratio		
Eo	Eötvös number, Eq. (7)		
F	force	N	
f	detachment frequency	Hz	
g	gravity acceleration	$m{\cdot}s^{-2}$	
K_{HR}	Hadamard reduction factor, Eq. (10)		
M	Morton number, Eq. (8)		
p	pressure	Pa	
Q_{in}	gas volumic flowrate	$mm^3{\cdot}s^{-1}$	
R	radius	m	
r	radius of curvature of cap	m	
Re	bubble Reynolds number, Eq. (6)		
s	distance between two consecutive bubbles	m	
Sr	Strouhal number, Eq. (27)		
T	temperature	°C, K	
t	time	s	
u	velocity	$m{\cdot}s^{-1}$	
V	volume	m^3	
We	Weber number, $= \rho u_B^2 d_{eq}/\sigma$		
x	horizontal coordinate (parallel to tube)	m	
y	vertical coordinate	m	
δ_i	error in measurement i		
γ	bubble distortion factor		
Θ	integer number of half periods	s	
λ	oscillation wavelength	m	
μ	dynamic viscosity	$Pa{\cdot}s^{-1}$	
ν	frequency of shape oscillations	Hz	
ρ	density	$kg{\cdot}m^{-3}$	
ρ'	reduced density, $= (\rho_l - \rho_g)/\rho_l$		
σ	surface tension	$N{\cdot}m^{-1}$	
χ	filter function		

Suffixes

B	bubble
D	drag
eq	equivalent
g	gas
G	center of gravity
in	inlet
l	liquid
max	maximum
med	mean
R	Rayleigh (frequency of)
T	terminal

u_B can be assumed as the total velocity of the bubble and F_D as the drag force exerted on it. Semi-empirical constitutive models are necessary to represent the terms C_M (virtual mass coefficient), and F_D (drag force). Generally C_M is given as 0.5 for a sphere in a fluid and 11/16 for a sphere attached to a plane [22]. When the bubble has reached its terminal velocity, or whenever the inertial contribution can be neglected, the former equations reduces to

$$F_D = (\rho_l - \rho_g) V_B g \tag{2}$$

Several models have been developed for the drag force, which can be expressed as [18]

$$F_D = C_D \frac{\pi d_{eq}^2}{4} \frac{\rho_l u_B^2}{2} \tag{3}$$

where C_D is the drag coefficient and d_{eq} is the bubble equivalent diameter, i.e., the diameter of the sphere having the same volume as the bubble

$$d_{eq} = \sqrt[3]{\frac{6V_B}{\pi}} \tag{4}$$

By substituting Eqs. (3), (4) in Eq. (2), the terminal velocity of the bubble can be derived as

$$u_{B,T} = \sqrt{\frac{4\rho' g d_{eq}}{3C_D}} \tag{5}$$

According to Clift et al. [18] and to Tomiyama et al. [17] the value of C_D can be correlated by Reynolds, Eötvös and Morton numbers:

$$Re = \frac{\rho_l u_B d_{eq}}{\mu_l} \tag{6}$$

$$Eo = \frac{(\rho_l - \rho_g) g d_{eq}^2}{\sigma} \tag{7}$$

$$M = \frac{(\rho_l - \rho_g) g \mu_l^4}{\sigma^3 \rho_l^2} \tag{8}$$

Alternatively, the Weber number ($We = \rho u_B^2 d_{eq}/\sigma$) could be adopted, though its use is generally more common for drops than for bubbles.

Three different regimes of terminal velocity of an isolated bubble can be distinguished as follows.

(1) A first region (viscosity-dominated), for very low Reynolds number, in which bubbles are spherical, viscosity forces dominate the terminal motion and terminal velocity increases with diameter.
(2) An intermediate region (surface-tension-dominated), in which surface tension and inertia forces determine the terminal velocity. Bubbles are no more spherical in this region and terminal velocity may either increase,

remain constant or decrease with equivalent diameter. According to Clift et al. [18], at least for air–water systems this regime holds for about $0.25 < Eo < 40$, however the boundaries (especially the lower one) are somewhat arbitrary [23].

(3) A last region (inertia-dominated), for high *Eo*, in which the bubbles are spherical-cap or bullet-shaped and the motion is dominated by the inertia forces. Velocity increases with equivalent diameter in this regime.

Besides, a distinction has been made among slightly contaminated or fully contaminated systems, in which, due to the accumulation of surfactants, the interface tends to behave as a rigid one and pure systems, in which the liquid-gas interface does not behave as a solid body. The latter bubbles show a reduced drag due to internal circulation, which reduces skin friction, and to the shifting backwards of boundary layer separation.

In the viscosity-dominated region, a number of relationship for C_D has been proposed in the general form

$$C_D = \frac{A_1}{Re} + \frac{A_2}{Re^m} + A_3 \tag{9}$$

Some of the proposed coefficients are reported in Table 1. The accuracy is in the order of 5%. More sophisticated expressions have been proposed as well. They are extensively treated by Clift et al. [18, Chapter 5].

The Hadamard–Rybczynski [26] reduction factor

$$K_{HR} = \frac{1 + \mu_g/\mu_l}{2/3 + \mu_g/\mu_l} \tag{10}$$

has also been used to divide the calculated values of C_D for a rigid sphere, in order to use them for pure systems, though rigorously this correction can be applied to the Stokes' law only. For gas-liquid systems, in which $\mu_l \gg \mu_g$, K_{HR} reduces to 1.5. This correction leads to overestimate C_D for $Re > 20$ [18, Chapter 5].

In the third region, according to [18], the model by Davies and Taylor [27] gives an accurate prediction of terminal velocity. After manipulation, it results in an expression of the drag coefficient (defined by Eqs. (3) and (5)) given by

$$C_D = 3\frac{d_{\text{eq}}}{r} \tag{11}$$

where r is the radius of curvature of the spherical cap. Since for $Re > 150$ the bubble becomes a spherical cap with a wake angle of approximately 50° [18], after some manipulation $d_{\text{eq}}/r \cong 0.89$ is found, which gives $C_D = 8/3$. This value is advised for $Re > 150$, $Eo > 40$ in [18, Chapter 8]. Extension to ellipsoidal cap can be found in the same reference.

In the intermediate region, models were proposed by Ishii and Chawla [28]

$$\begin{aligned} C_D &= \frac{2}{3}\sqrt{Eo} \quad (Eo < 16) \\ C_D &= \frac{8}{3} \qquad\quad (Eo \geqslant 16) \end{aligned} \tag{12}$$

and by Tomiyama et al. [17]

$$C_D = \frac{8}{3}\frac{Eo}{Eo + 2B_4} \tag{13}$$

where $B_4 = 2$ was originally proposed for air–water (adiabatic) systems, though $B_4 = 2.4$ seems to give better results for air bubbles in pure stagnant water [21].

Wallis [29] has noted that in the past several authors have identified a part of this region as characterized by a constant value of Weber number: e.g., Peebles and Garber [1] proposes $We = 3.65$ for bubbles. By simple manipulation this condition results in $C_D = \text{const} \cdot Eo$. Wallis proposes $We = 4$ and this results in $C_D = Eo/3$.

Tomiyama et al. [17] reconsidered former approaches and developed a general correlation for C_D, valid throughout all the regions above, which fitted nicely the available experimental data and can be expressed in the general form

$$C_D = \max\left\{\min\left[\frac{B_1}{Re}\left(1 + 0.15Re^{0.687}\right), \frac{B_2}{Re}\left(1 - B_3 Re^{-0.5}\right)\right], \frac{8}{3}\frac{Eo}{Eo + 2B_4}\right\} \tag{14}$$

where the coefficients B_i assume different values according the nature and the contamination of the system, see Table 2. This model has recently extended by Celata et al. [21] in order to fit refrigerant data and the corresponding coefficients are reported as well.

Table 1
Coefficients in Eq. (9)

A_1	A_2	A_3	m	Ref.	Remarks
24	0	0	0	[24]	Classical Stokes' law, rigid sphere, $Re < 1$
24	0	0	0.188	[24]	Oosen solution, rigid sphere, $Re < 5$
24	3.6	0	0.313	[18]	Schiller and Nauman, rigid sphere, $Re < 800$,
48	0	0	0	[25]	Levich, pure system, $Re > 100$,
48	−106.1	0	1.5	[18]	Moore, pure system, $20 < Re < 1000$
72	0	0	0	[17]	Levich, slightly cont. system
24	2.4	0	0.25	[17]	Ishii and Chawla
0	18.7	0	0.68	[1]	Peebles and Garber

Table 2
Coefficients in Eq. (14)

B_1	B_2	B_3	B_4	Ref.	Remarks
16	48	0	2	[17]	Pure adiabatic system
24	72	0	2	[17]	Slightly contaminated ad. syst.
24	∞	0	2	[17]	Fully contaminated ad. system
16	48	2.21	5	[21]	FC-72, diabatic system
16	48	2.21	4	[21]	R-114, diabatic system

As reported in [17], comprehensive expressions of the same kind as Eq. (14), can be derived also from the work of Ishii and Chawla [28]

$$C_D = \max\left\{\frac{24}{Re}\left(1 + 0.1Re^{0.75}\right), \min\left[\frac{2}{3}\sqrt{Eo}, \frac{8}{3}\right]\right\} \tag{15}$$

and by Peebles and Garber [1]

$$C_D = \max\left\{\max\left[\frac{24}{Re}, \frac{18.7}{Re^{0.68}}\right], \min\left[0.0275Eo\,We^2, 0.82Eo^{0.25}We^{0.5}\right]\right\} \tag{16}$$

In this equation, $Eo\,We^2$ has been used in place of the original Re^4M in order to stress that the terminal velocity does not depend on viscosity in the second and third region (viscosity cancels out in the product Re^4M). Peebles and Garber [1] noted also that the rightmost expression implies a terminal velocity independent of bubble diameter, which is in contrast with Davies and Taylor model, Eq. (11).

A general correlation for bubble velocity has been proposed by Wallis too [29]. He distinguished among five regions (some of them subdivided in sub-regions) correlating the data with simple relationships containing a dimensionless velocity v^* and a dimensionless radius r^*. By recasting his expressions for fluid spheres, the following relationship is achieved

$$C_D = \max\left\{\min\left[\max\left(\frac{16}{Re}, \frac{13.6}{Re^{0.8}}\right), \frac{48}{Re}\right], \min\left[\frac{Eo}{3}, 0.47Eo^{0.25}We^{0.5}, \frac{8}{3}\right]\right\} \tag{17}$$

According to the models above, the shape of the bubble does not play an independent role on its terminal velocity, i.e., it is assumed to be a single-value function of Re, M, Eo. Very recently, Tomiyama et al. [30] provided experimental evidence that this is not true, at least in the intermediate region of terminal velocity. Consequently, they proposed a new model which includes the bubble shape as an independent parameter. This new model can be considered as an extension of Davies and Taylor approach to the surface-tension-dominated region and it is supported by experimental data for an air–water system. The bubble is assumed to be a distorted oblate spheroid, so that two new parameters are introduced: the aspect ratio E (i.e., the ratio between minor and major axes of the bubble) and the distortion factor γ, whose value ranges from 1, for an ellipsoid, to 2, for a hemispheirodal cap bubble. In the assumption that the potential flow region is restricted to the bubble tip, the following expression of C_D results

$$C_D(Eo, \gamma, E) = \frac{2Eo}{\gamma E^{3/2}(1 - \gamma^2E^2)Eo + 16\gamma E^{4/3}}\left[F(\gamma E)\right]^{-2} \tag{18}$$

where

$$F(z) = \frac{\sin^{-1}\sqrt{1 - z^2} - z\sqrt{1 - z^2}}{1 - z^2} \tag{19}$$

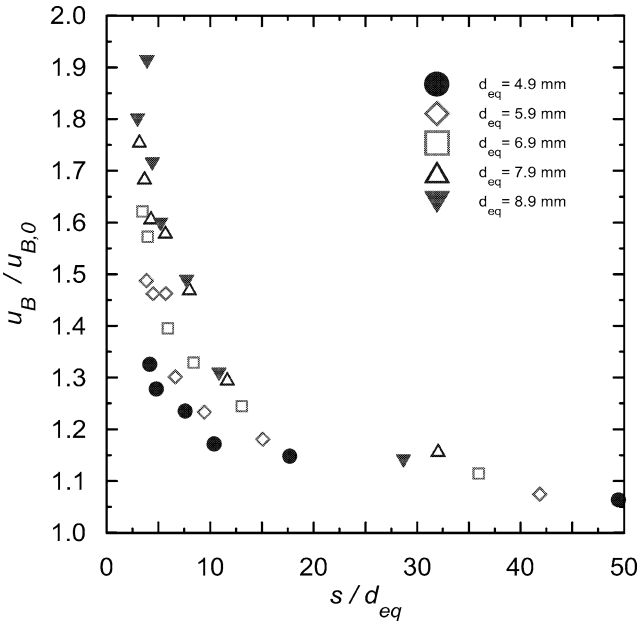

Fig. 1. Terminal velocity of bubbles in train (normalized to the one of an isolated bubble) vs. dimensionless bubble spacing, adapted from Tsuge and Hibino [9].

This expression can be recognized as a modified version of Eq. (13) in which the coefficients are made dependent on γ and E.

So far, the interaction between succeeding bubbles in a column has been neglected. Tsuge and Hibino [9] reported data of large bubbles rising in water ($d_{\text{eq}} = 5{-}9$ mm) at different detaching frequencies, which have been re-plotted as a function of dimensionless spacing between bubbles, s/d, in Fig. 1. Here, the increase of terminal velocity with reducing s/d may be interpreted as a wake effect, which is increasing with bubble diameter.

Finally, it is worth stressing that, while a considerable amount of research was devoted to the drag forces acting on a bubble rising in a still liquid, far less attention has been paid on the lift forces, which are responsible of the oblique, zig-zag or helical motions so often encountered in experiments. These motions are generally attributed to wake shedding.

2. Experimental apparatus

Adiabatic two-phase flow conditions were established by injecting gas bubbles in a liquid through an orifice. The experimental cell consisted of an aluminum box of about 2.5 dm^3 volume, monitored by temperature and pressure sensors (see Fig. 2). The cell was provided with windows on two sides and on the upper part, to allow visualization and video shots of phenomena occurring inside. The working fluid was FC-72 (C_6F_{14}) a fluoroinert liquid manufactured by 3M, used in electronics cooling. The geometry of the test section was derived from the one of an analogous apparatus

operated at Pisa University, to study boiling phenomena [31], in order to compare the results. It consisted mainly of an horizontal copper tube (1 mm o.d. 0.2 mm i.d.) connected to the gas injection device. The nitrogen was injected from a pressurized vessel into the fluid via a circular orifice (0.13 mm diameter) drilled in the upper part of the tube. An electric field could also be generated by imposing a d.c. potential drop to a 8-rod cylindrical squirrel cage surrounding the tube. Though the rods were left in place, this feature was not utilized for obtaining the results described herein. The facility was intended for operation in microgravity conditions too [32]. To this aim, the fluid container was connected to bellows in order to allow for volume dilatation due to temperature changes and gas injection, without leaving a free surface above the liquid.

To measure and control nitrogen mass flow a digital mass flow controller (model El-Flow by Bronkhorst) was used in each cell: this device guaranteed a stable inlet flow (proportional to an input voltage) in the chamber below the orifice. The outlet flow rate from the orifice stabilized at the same value within some seconds. The apparatus was intended to work in "fixed flow" conditions; these were achieved mainly by reducing the volume of the gas chamber under the orifice. The conditions to ensure "fixed-flow" operation are discussed in detail by Danti et al. [33].

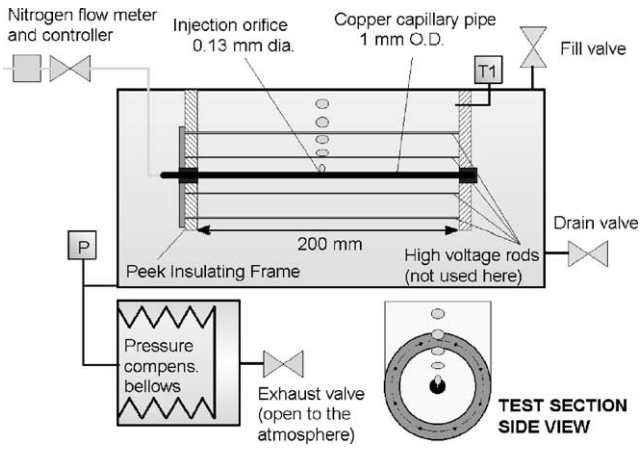

Fig. 2. Experimental apparatus.

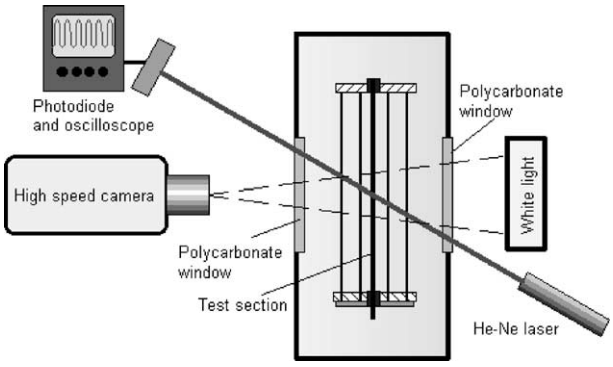

Fig. 3. Sketch of the optical setup.

During the experiments reported herein, measurements of bubble volume, aspect ratio and velocity were taken by digital processing of video images taken with a high speed camera (Phantom V4.0 by Vision Researchs) at a frame rate of 1500 fps and with a resolution of about 20 pixel·mm^{-1}. The detachment frequency was measured by analyzing the signal of a photodiode hit by a He–Ne laser beam, which was intersected by the rising bubbles, as this method is more convenient, fast and accurate than the use of the high speed camera. The optical arrangement is sketched in Fig. 3.

The data reduction procedure and the related uncertainties are reported in Appendix A. Typical uncertainties in equivalent diameter and aspect ratio measurement were around 2%, and those in velocity (for a single bubble) ranged from 3% to 4.5%.

3. Results and discussion

In this work, values of rising velocity of bubbles were measured in a wide range of detachment frequency and volume. This was achieved by varying the inlet gas flowrate from 1.5 to 53 mm^3·s^{-1}. All the tests were carried out at atmospheric pressure (105 ±3 kPa) and in a range of fluid temperature from 21 to 26 °C. In this range, the viscosity of FC-72 varies from 0.68 to 0.63 mPa·s (3M Handbook, [34]). The Morton number M ranged from 7.19×10^{-10} to 8.41×10^{-10}, Re from 300 to 450, and Eo from 0.7 to 1.4.

3.1. Detachment diameter and frequency

The detachment diameter vs. the flowrate followed a characteristic trend reported in Fig. 4. The plot of detachment frequency is reported in Fig. 5.

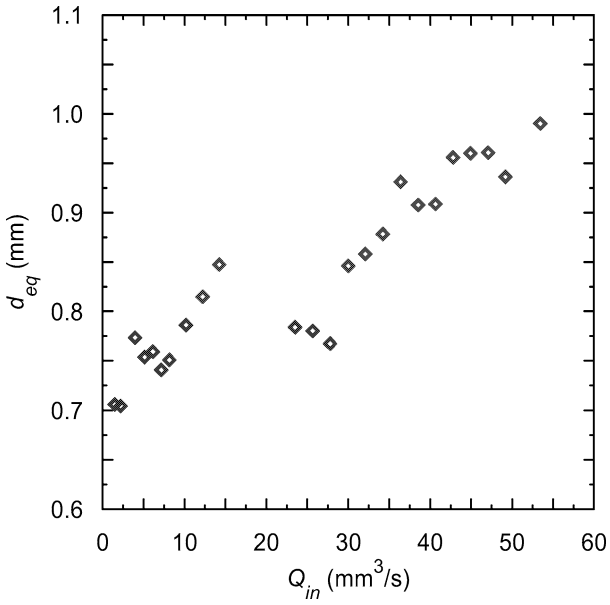

Fig. 4. Bubble detachment diameter vs. inlet flowrate.

It is worth noting that in the range $16 < Q_{\text{in}} < 22\ \text{mm}^3\cdot\text{s}^{-1}$ the detachment occurred steadily with two different alternating periods and diameters, so that the corresponding data were omitted from this study. This is evident from Fig. 6, where the flow patterns at different flowrates are depicted. These data are in agreement with former ones obtained with the same apparatus and the dependence of the detachment volume on gas flowrate has already been analyzed [33].

3.2. Velocity and aspect ratio

The typical evolution of bubble velocity with distance from the orifice is reported in Fig. 7: after an initial acceleration, and as long as bubble path keeps vertical or nearly vertical, the velocity oscillates around a constant value; this defines the measurement region for the rising velocity.

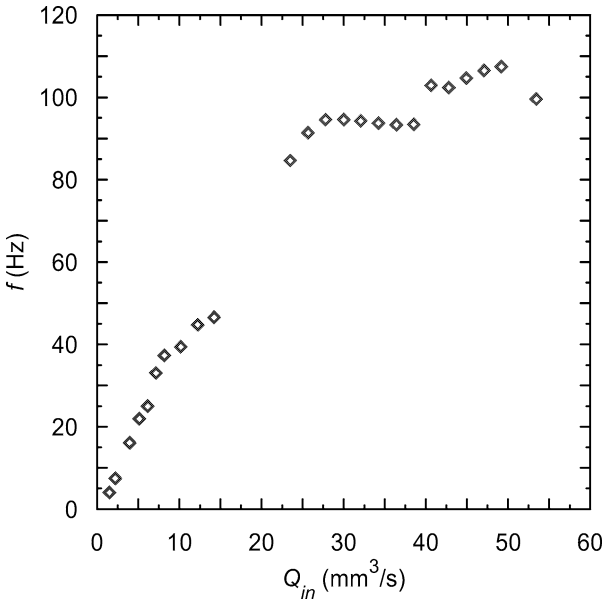

Fig. 5. Bubble detachment frequency vs. inlet flowrate.

The periodic oscillation of rising velocity was almost identical for a number of consecutive bubbles. It exhibited a definitely non-stochastic nature and its amplitude was markedly greater than the experimental uncertainty. This oscillation was also well correlated with the oscillation of aspect ratio: the two measurements are reported together in Figs. 8–10 for three different values of flowrate: the oscillations are almost in phase, with a very small delay for velocity peak. The correlation becomes more and more evident with increasing inlet gas flowrate. This is also well evidenced in Fig. 11, where the two measurements are reported one vs. the other, after normalization as follows

$$u_{\text{norm}} = \frac{u_B - \bar{u}_B}{u_{B,\max} - \bar{u}_B} \tag{20}$$

$$E_{\text{norm}} = \frac{E - \overline{E}}{E_{\max} - \overline{E}} \tag{21}$$

The mean aspect ratio is reported vs. *Eo* in Fig. 12 together with a correlation by Welleck et al. [35], valid for $Eo < 40,\ M < 10^{-6}$, as reported

$$\overline{E} = \frac{1}{1 + 0.163 Eo^{0.757}} \tag{22}$$

where $\overline{E}$ is ensemble averaged and *Eo* is calculated using d_e. It can be seen that the measured values ($0.55 < E < 0.7$) are overestimated by the correlation. On the other hand, the same disagreement was encountered in [18] for a pure system.

3.3. Shape oscillations

The frequency of shape oscillations can be derived from

$$\nu = \frac{\bar{u}_{B,T}}{\lambda} \tag{23}$$

where λ is the spatial distance between two consecutive maxima in E, taken from the plots (i.e., the spatial wavelength). Shape oscillations were not detectable for $Q_{\text{in}} <$

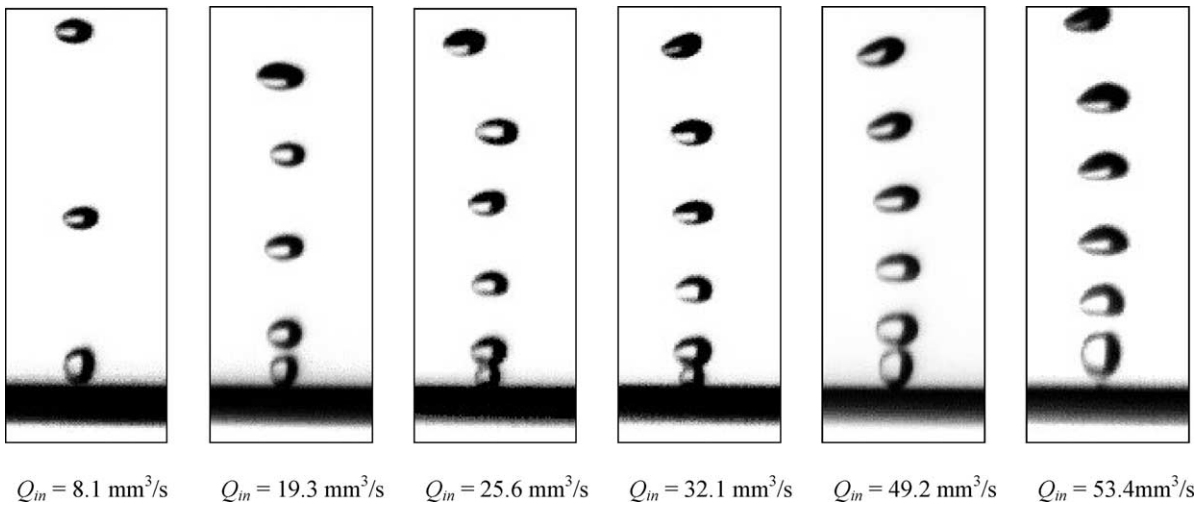

Fig. 6. Bubble flow patterns at different values of inlet flowrate. The thickness of the pipe (black line at the bottom) is 1 mm.

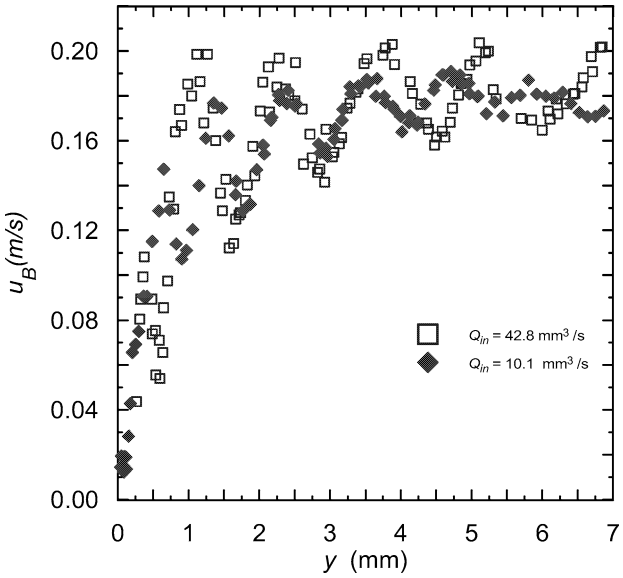

Fig. 7. Typical trend of bubble velocity vs. distance from the orifice.

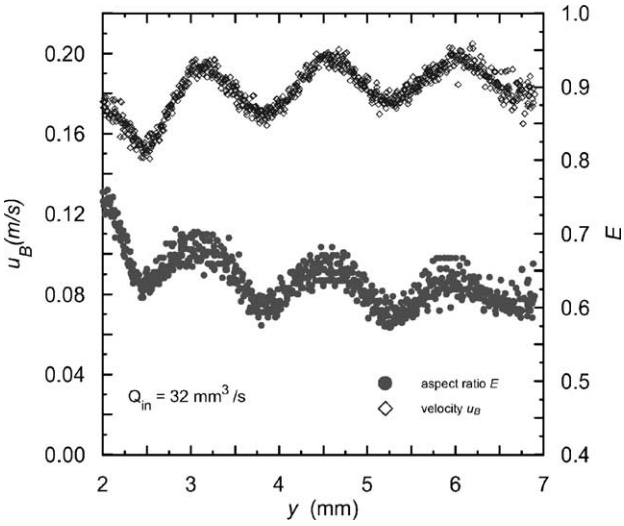

Fig. 8. Trend of terminal velocity and aspect ratio vs. distance from the orifice.

5 mm^3·s^{-1}, presumably due to the insufficient length resolution of the camera. The data were compared in Fig. 13 with the well-known Rayleigh equation [36] for the first mode of shape oscillation of a spherical bubble

$$\nu_R = \frac{1}{2\pi}\sqrt{\frac{192\sigma}{(2\rho_l + 3\rho_g)d_{\text{eq}}^3}} \tag{24}$$

Eq. (24) overestimates the oscillation frequency. This was expected, as in [18] discrepancies up to 40% for pure systems are reported. The introduction of a damping coefficient, as proposed, e.g., in [37,38] did not introduce a significant variation of the calculated frequencies.

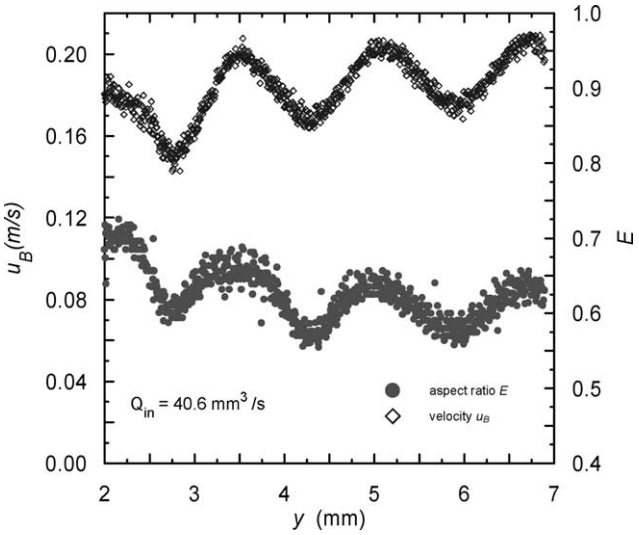

Fig. 9. Trend of terminal velocity and aspect ratio vs. distance from the orifice.

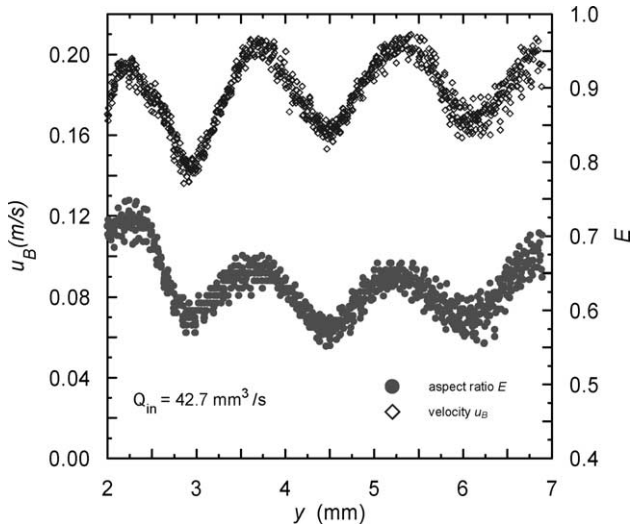

Fig. 10. Trend of terminal velocity and aspect ratio vs. distance from the orifice.

Edge and Grant [39], provided an empirical model, though in dimensional form, for liquid drops into liquid

$$\nu = \nu_R - 26.5\frac{1}{\rho'^{0.2}}\left(\frac{1.62}{d_{\text{eq}}(\text{mm})}\right)^2 \tag{25}$$

Schroder and Kintner [40] proposed a correction of Eq. (24) based on the amplitude of oscillations

$$\nu = \nu_R\sqrt{1 - \frac{c_{\max} - c_{\min}}{2c_{\text{med}}}} \tag{26}$$

where c is the size of the bubble in the direction of motion. From Fig. 13, it can be noted that Eq. (25) slightly overestimates the frequency data, while the correction given by Eq. (26) is not sufficient to fit data.

In conclusion, none of the proposed models fitted the experimental data satisfactorily. Actually, it must be noted that the Rayleigh's model refers to the shape oscillations of

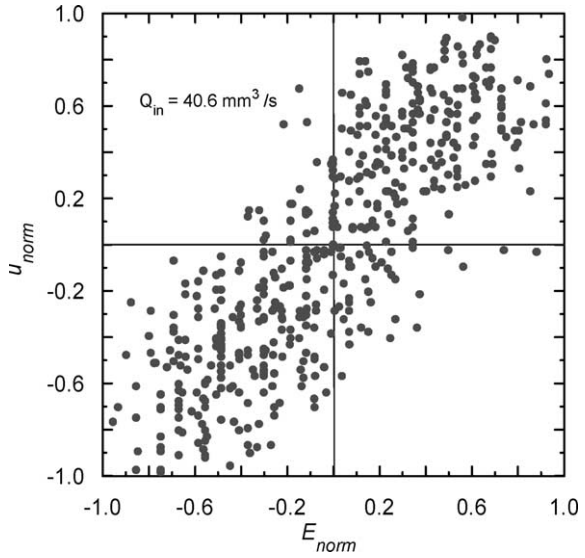

Fig. 11. Normalized bubble velocity vs. normalized aspect ratio for $Q_{\text{in}} = 40.6\ \text{mm}^3\cdot\text{s}^{-1}$.

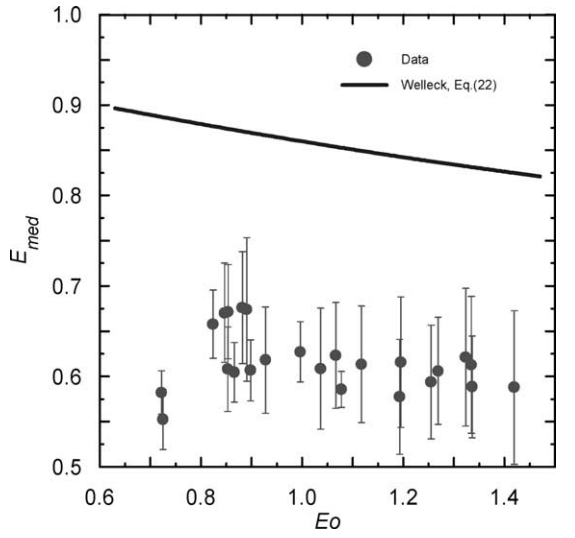

Fig. 12. Mean aspect ratio vs. *Eo* and comparison with correlation by Welleck.

quiescent spherical drops in a still liquid: neither the effect of bubble motion is accounted for, nor the fact that the bubble is elliptical in the present case. Besides, the present oscillation were of the kind oblate–less oblate, and not oblate–prolate.

Some authors [39] also suggest that the shape oscillations of a bubble may be forced by vortex shedding from its surface: this observation may be supported by the fact that the Strouhal number of the bubbles

$$Sr = \frac{\nu d_{\text{eq}}}{\bar{u}_{B,T}} \tag{27}$$

tended to assume a constant value, around 0.6 in our case (see Fig. 14). This value is quite close to the typical *Sr* related to vortex shedding, which is generally less than unity. On the other hand, the shape oscillations could be simply due

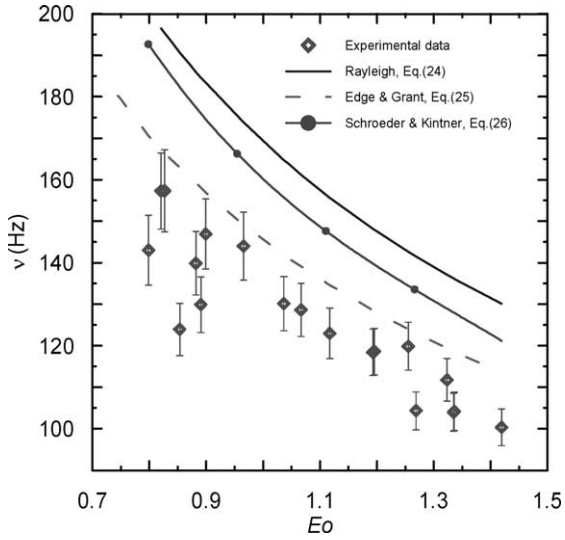

Fig. 13. Bubble shape oscillation frequency vs. equivalent diameter and comparison with available models.

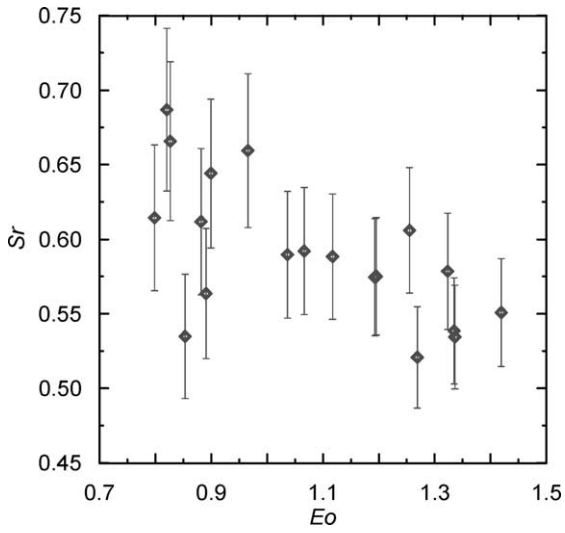

Fig. 14. Bubble Strouhal number vs. *Eo*.

to the perturbations originated by bubble detachment. The whole matter clearly needs a more thorough assessment.

3.4. Rising mean velocity and comparison with available correlations

The mean rising velocity is defined as

$$\bar{u}_{B,T} = \frac{1}{\Theta}\int_0^{\Theta} u_B \,\mathrm{d}t \tag{28}$$

where Θ represents an integer number of half-periods in the measurement region. It was evaluated as reported in Appendix A and it is plotted vs. *Eo* in Fig. 15 after ensemble averaging. The amplitude of oscillation of rising velocity is also evidenced in the same figure, where the maximum and minimum values are reported as well. From the figure it can

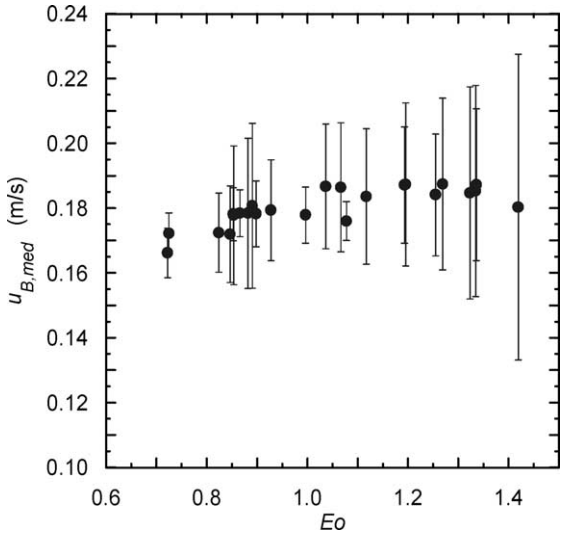

Fig. 15. Mean terminal velocity vs. *Eo*. Bars represent amplitude of velocity oscillation and not uncertainty bands.

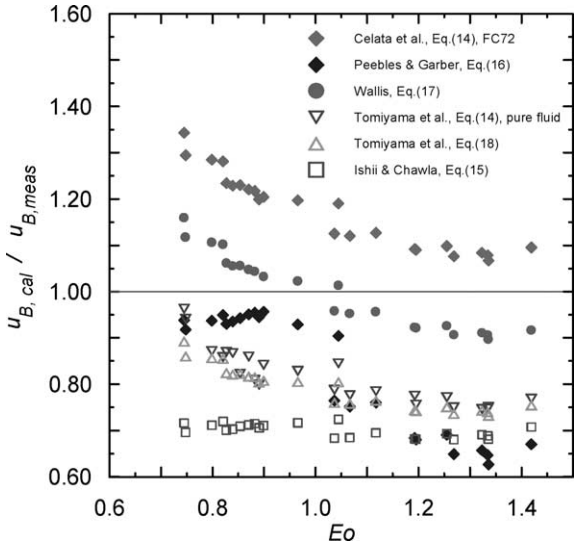

Fig. 16. Mean terminal velocity: comparison with predictions of available models.

be noted that such oscillation may reach 20% of the mean value. This implies that local measurements taken at a single position might be highly misleading.

In the presence of so wide velocity oscillations, one may wonder if the acceleration term (LHS in Eq. (1)) is really negligible. The maximum acceleration can be estimated as the amplitude of the first harmonic in a Fourier expansion of the velocity as

$$u'_{\max} = 2\pi\nu A_u \tag{29}$$

and the ratio of the acceleration to buoyancy can be evaluated from Eq. (1) as

$$a' = \frac{C_M 2\pi\nu A_u}{\rho' g} \tag{30}$$

For the present experimental data, a' ranged from 0.4 to 1.4 (using $C_M = 0.5$), thus demonstrating that some influence of the acceleration term can be found also in terminal motion, though this effect has been often discounted in the past.

Nonetheless, a simpler relationship can be retained with some assumptions. By integrating Eq. (1) over an integer number of half-periods, and by assuming C_D independent of bubble velocity and aspect ratio (this is the case if an expression like Eq. (13) holds) one gets

$$\int_0^{\Theta} V_B \frac{\mathrm{d}}{\mathrm{d}t}\left[(\rho_g + C_M\rho_l)u_B\right]\mathrm{d}t = (\rho_l - \rho_g)V_B g\Theta - C_D\frac{\pi d_{\mathrm{eq}}^2}{4}\frac{\rho_l}{2}\int_0^{\Theta} u_B^2\,\mathrm{d}t \tag{31}$$

Since the LHS vanishes the following expression is obtained

$$(\rho_l - \rho_g)V_B g - C_D\frac{\pi d_{\mathrm{eq}}^2}{4}\frac{\rho_l}{2}\bar{u}_{B,T}^2 = 0 \tag{32}$$

where $\bar{u}_{B,T}^2$ is the mean square velocity. Eq. (32) can be rearranged as Eq. (5). In the tested conditions, its difference from the mean rising velocity was less than 1%. Extension to the case in which C_D depends on velocity can also be performed. In this way, the measured mean rising velocity can be compared with the predictions of the available models for terminal velocity with reasonable accuracy. The results are shown in Fig. 16: it can be seen that none of the available models is able to satisfactorily predict the experimental outcomes. The general trend is to underpredict the rising velocity, except for the model explicitly derived for FC-72 (though in diabatic flow conditions) which overestimates the experimental data, and for the Wallis correlation which overpredicts the data at low *Eo*. Besides all the models tend to predict lower velocities with increasing *Eo*, with the only exception of the model of Ishii and Chawla, which gives a "flat" trend, though with a marked underprediction. A comparison with the model accounting explicitly for bubble aspect ratio, Eq. (18), has also been performed, assuming that E can be replaced by its mean value and $\gamma = 1$. It does not seem to improve significantly the results, at least with the assumptions made. It must be also noted that wall effects can be excluded, as the cell is about 100 bubble diameters wide [18].

Finally, the mean rising velocity was normalized to the one of the bubble detaching with the lower frequency, and is plotted vs. the dimensionless bubbles spacing in Fig. 17, in order to assess the presence of a wake effect. It can bee seen that the increase of velocity at lower values of bubble spacing is below 10%. It should be also remarked that, contrary to Fig. 1, the present data are not referred to the same bubble diameter. In fact, there was no possibility to control the detachment diameter independently of detachment frequency in the present apparatus. Since the bubble diameter is increasing with frequency (see Figs. 4 and 5) and the rising velocity increases with diameter (see

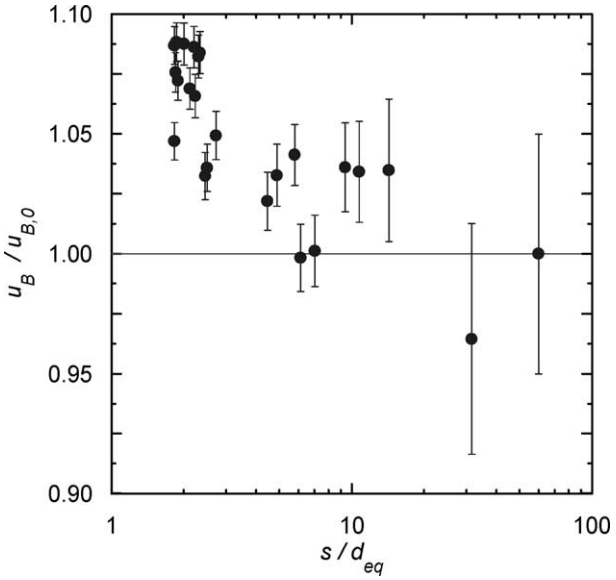

Fig. 17. Mean terminal velocity (normalized to the one of the bubble detaching with the lowest frequency) vs. dimensionless bubble spacing.

Fig. 15), the increase in velocity at the low values of s/d could be simply caused by these effects. Anyway, it can be concluded that in the tests performed herein the wake effect is very low or negligible. On the other hand, the increase in velocity measured by Tsuge and Hibino, see Fig. 1, could be due to the larger diameter of the bubbles, to the higher viscosity of water, or even to totally different reasons, for example linked to the way in which bubbles are generated. Considering Fig. 17, it must be noted that Clift et al. [18] report that the bubble wake extends no more than two diameters: thus, bubbles detaching at low frequency can be considered isolated.

4. Conclusions

An experimental apparatus was set up and operated to study gas bubble dynamics. In order to separate the mechanical effects from the thermal and mass exchange ones, adiabatic two-phase flow conditions were established by injecting nitrogen gas bubbles in a fluoroinert liquid through an orifice. The geometry of the test section and of the electric field was chosen in order to allow a future comparison with the results of a similar apparatus operated by the LOTHAR laboratory of the University of Pisa and dedicated to the investigation of boiling phenomena. Bubble size, aspect ratio, detachment frequency, velocity and frequency of shape oscillations were measured.

The present findings showed that, after an initial acceleration region, the bubble did not reach a steady state conditions, but rather a periodical one in which significant shape and velocity oscillations persisted. In the same region, due to the velocity oscillation, the influence of acceleration term (LHS in Eq. (1)) was still significant, so that instantaneous force balance should account for it. There is no evidence that this rising regime can continue indefinitely, at least due to the bubble expansion caused by the decrease in hydraulic head along large distances. The oscillations of shape and velocity were well correlated, thus providing further experimental evidence that the drag coefficient does not depend on the equivalent diameter only, but it has a separate dependence on the aspect ratio too. The available correlations were not able to provide a fully satisfactory prediction of the average value of the rising velocity and tended to underestimate it, especially for the higher values of *Eo*. By analyzing the trend of velocity as a function of the dimensionless bubble spacing, the presence of a significant wake effect could be excluded.

To a deeper insight, the concept itself of "terminal velocity" of a bubble probably needs reconsideration: likely the bubble remains an entity in dynamical evolution and may present different values of "terminal" velocity along its path, depending on its past history and on surrounding conditions. Simple correlations, like the ones presented in Section 1, may give at most a hint in evaluating it.

The frequency of shape oscillations was overestimated, as expected, by the classical Rayleigh model. Corrections of this model available in literature did not provide satisfactory results. It was also observed that the bubble Strouhal number, *Sr*, tended to assume a constant value around 0.6.

Acknowledgements

Thanks are due to Mr. Roberto Manetti for the design and the assembling of the electronics and for technical assistance. The fruitful discussions with Dr. Gian Piero Celata and Prof. Akio Tomiyama are gratefully acknowledged.

The work was funded by the Italian Ministry of Education, University and Research (MIUR) under the National Interest Project n. 39 for the year 2000.

Appendix A. Data reduction and measurement uncertainties

The detachment frequency comes from the period, defined as the temporal distance between two completely detached bubbles, measured from the peak signal on the oscilloscope. The reported value is a mean over ten measurements and error was calculated as the sum of the two contributions:

$$\Delta f = \frac{\sqrt{\delta_t^2 + \sigma_t^2}}{T_0^2} \tag{A.1}$$

where $\delta_t = 0.02$ ms is oscilloscope resolution and σ_t is the sample standard deviation over the measurements, which is usually larger.

The measurements taken from the video images for this study are center of mass velocity, bubble equivalent diameter

and aspect ratio. From these measurements mean quantities like rising velocity, aspect ratio and oscillation frequency are derived.

Time measurements with the camera are affected by one frame resolution, which corresponds to $\delta_t = 0.66$ ms for 1500 fps. For each value of the gas flow the camera recorded 0.2 s, showing a number of bubbles M depending on the detachment frequency (from 3 to 30). For the lower values of frequency the recorded time was enlarged, so to consider at least 3 bubbles.

Image processing was then performed using a free-ware software (Scion Image), working with binary images.

A threshold method was used for edge detection (after contrast enhancing). The brightness histogram showed two peaks corresponding to the background and the gray level typical of the bubbles. The threshold level was chosen in midway between the two peaks. This method was tested with good results on spherical and elliptical objects of known volume and permits to measure N (number of pixels in a bubble) and p (number of pixels in its perimeter). The center-of-mass coordinates of a bubble were defined as

$$\begin{aligned} x_G &= \frac{1}{N}\sum_i\sum_j x_i\psi(x_i, y_j) \\ y_G &= \frac{1}{N}\sum_i\sum_j y_i\psi(x_i, y_j) \end{aligned} \tag{A.2}$$

where x and y are pixel coordinates (y axis in the gravity direction) and $\psi(x, y)$ is a function whose value is 1 if (x, y) is in the considered bubble and 0 elsewhere.

The error on these measurements is mainly due to lines/columns counting: if the bubble is enclosed in a rectangular frame whose dimension in pixels are a (y direction) and b (x direction), the uncertainties in the coordinates center of mass are $\delta_{y_G} = 1/\sqrt{b}$ and $\delta_{x_G} = 1/\sqrt{a}$.

The vertical velocity is obtained from two frames (not necessarily two consecutive ones) taken at times t_1 and t_2

$$u = (y_{G2} - y_{G1})/(t_2 - t_1) \tag{A.3}$$

This value is assigned at the point whose vertical coordinate is $y = (y_{G2} + y_{G1})/2$, and errors are thus calculated by propagation as

$$\left(\frac{\Delta u}{u}\right)^2 = \frac{\delta_{x_{G2}}^2 + \delta_{x_{G1}}^2}{(y_{G2} - y_{G1})^2} + \frac{\Delta t_1^2 + \Delta t_2^2}{(t_2 - t_1)^2} \tag{A.4}$$

For a fixed value of the gas flow different bubbles followed a similar trajectory, which is rectilinear up to a certain distance from the orifice. This permitted to take, for any position y, an ensemble average $\bar{u}$ over the M recorded bubbles, which describes the behavior of the "typical bubble" passing there, for a fixed value of the gas flow. The error on this quantity was taken as $\Delta u/\sqrt{M-1}$.

The mean rising velocity u_T is evaluated as a mean over the K measurements taken:

$$\bar{u}_{B,T} = \frac{\sum_j^K u_j \chi(Q_{\text{in}}, y_j)}{\sum_j^K \chi(Q_{\text{in}}, y_j)} \tag{A.5}$$

where j is an index that runs over the K measurements and $\chi(Q_{\text{in}}, y_j)$ is a function whose value is 1 in the measurement region and 0 elsewhere. Due to the presence of periodic variations of the velocity with orifice distance, the mean value u_T must be calculated over an integer number of half-periods, to weight these oscillations equally. This consideration was included in the definition of the function $\chi(Q_{\text{in}}, y_j)$ for a fixed value of Q_{in}.

The volume of the bubble is evaluated as

$$\begin{aligned} V &= 2/3 \cdot (\text{projected area}) \cdot (\text{max axis}) \\ &= 2/3 \cdot (N - p/2 - 1) \cdot (b - 1) \end{aligned} \tag{A.6}$$

i.e., considering the contour passing in the middle of each perimetral pixel and bubbles as oblate ellipsoids with $b-1$ and $a-1$ as major and minor axis, respectively.

The calculated values showed a plateau in part of the terminal region; a mean over these values was taken as the detachment volume. The error was derived (considering $p/2$ as the area error) as

$$\Delta V = \frac{p}{2(N - p/2 - 1)} V \tag{A.7}$$

Finally, the equivalent diameter was obtained by Eq. (4) and the error on it from

$$\frac{\Delta d_{\text{eq}}}{d_{\text{eq}}} = \frac{1}{3}\frac{\Delta V}{V} \tag{A.8}$$

The hypothesis on the bubble shape, used in Eq. (A.6), also defines the aspect ratio E as:

$$E = \frac{a-1}{b-1} \tag{A.9}$$

The reported values of E were averaged on some (typically 3) consecutive measurements. The mean value for aspect ratio $\overline{E}$ was defined using the same spatial filter $\chi(Q_{\text{in}}, y_j)$ used for velocity $\bar{u}_{B,T}$, and ensemble-averaged over M bubbles.

The so obtained lengths are in pixels (velocities in pixel·s^{-1} and volumes in pixel^3); a conversion factor is needed to change them into metrical units. This was measured from a gauge image, taken before the test in the same optical conditions, featuring a steel bar with ticks at known distances and introduces in calculations a new source of errors to be propagated. This error was added at the final stage to the previous ones and is mainly statistical (due to mechanical differences in ticks, differences in the light distribution etc.).

Finally, the frequency of shape oscillations, ν, is a mean over the measurement region.

References

[1] F. Peebles, H. Garber, Studies on the motion of gas bubbles in liquid, Chem. Engrg. Prog. 49 (2) (1953) 88–97.

[2] J.F. Davidson, B.O. Schuler, Bubble formation at an orifice in an inviscid liquid, Trans. Inst. Chem. Engrg. 38 (1960) 335–342.

[3] J.F. Davidson, B.O. Schuler, Bubble formation at an orifice in a viscous liquid, Trans. Inst. Chem. Engrg. 38 (1960) 144–154.
[4] S. Ramakrishnan, R. Kumar, N.R. Kuloor, Studies in bubble formation—I. Bubble formation under constant flow conditions, Chem. Engrg. Sci. 24 (1969) 731–747.
[5] A. Satynarayan, R. Kumar, N.R. Kuloor, Studies in bubble formation—II. Bubble formation under constant pressure conditions, Chem. Engrg. Sci. 24 (1969) 749–761.
[6] A.K. Khurana, R. Kumar, Studies in bubble formation—III, Chem. Engrg. Sci. 24 (1969) 1711–1723.
[7] R. Kumar, N. Kuloor, The formation of bubbles and drops, Adv. Chem. Engrg. 8 (1970) 255–368.
[8] A.E. Wraith, Two-stage bubble growth at a submerged orifice, Chem. Engrg. Sci. 26 (1971) 1659–1671.
[9] H. Tsuge, S.I. Hibino, The motion of gas bubbles generating from a single orifice submerged in a liquid, Keio Engineering Reports 25 (7) (1972).
[10] I. Zun, J. Groselj, The structure of bubble non-equibrium movement in free-rise and agitated-rise conditions, Nucl. Engrg. Des. 163 (1996) 99–115.
[11] Y. Park, A. Lamont Tyler, N. de Nevers, The chamber orifice interaction in the formation of bubbles, Chem. Engrg. Sci. 32 (1977) 907–916.
[12] D. Bhaga, M.E. Weber, Bubbles in viscous liquids: Shape, wakes and velocities, J. Fluid Mech. 105 (1981) 61–85.
[13] J.R. Grace, T. Wairegi, T.H. Nguyen, Shapes and velocities of single drops and bubbles moving freely through immiscible liquids, Inst. Chem. Engrg. 54 (1976) 167–173.
[14] O. Pamperin, H.J. Rath, Influence of buoyancy on bubble formation at submerged orifices, Chem. Engrg. Sci. 50 (19) (1995) 3009–3024.
[15] Yu.A. Buyevich, B.W. Webbon, Bubble formation at a submerged orifice in reduced gravity, Chem. Engrg. Sci. 51 (21) (1996) 4843–4857.
[16] A. Tomiyama, Struggle with computational bubble dynamics, in: Proc. 3rd International Conference on Multiphase Flows (CD-ROM), Lyon, 8–12 June, 1998.
[17] A. Tomiyama, I. Kataoka, I. Zun, T. Sakaguchi, Drag coefficients of single bubbles under normal and microgravity conditions, JSME Internat. J. Ser. D 41 (2) (1998) 472–479.
[18] R. Clift, J.R. Grace, M.E. Weber, Bubbles, Drops and Particles, Academic Press, New York, 1978, p. 172.
[19] H. Tsuge, Hydrodinamics of bubble formation from submerged orifices, in: Encyclopedia of Fluid Mechanics, 1986, pp. 191–232, Chapter 9.
[20] G.P. Celata, M. Cumo, F. D'Annibale, A. Tomiyama, Terminal bubble rise velocity in one-component systems, in: 39th European Two-Phase Flow Group Meeting, Aveiro, Portugal, 18–20 June, 2001, Paper F-3, pp. 1–10.
[21] G.P. Celata, M. Cumo, F. D'Annibale, A. Tomiyama, Bubble rising velocity in saturated liquid up to the critical pressure, in: G.P. Celata, P. Di Marco, A. Goulas, A. Mariani (Eds.), Experimental Heat Transfer, Fluid Mechanics and Thermodynamics, 2001, pp. 1319–1328.
[22] L.M. Milne Thomson, Theoretical Hydrodynamics, 5th Edition, Dover, Mineola, NY, 1996.
[23] J.R. Grace, Shapes and velocities of bubbles rising in infinite liquids, Trans. Inst. Chem. Engrg. 51 (1973) 116–120.
[24] H. Schlichting, Boundary-Layer Theory, 7th Edition, McGraw-Hill, New York, 1979, p. 116.
[25] V.G. Levich, Physicochemical Hydrodynamics, Prentice-Hall, New York, 1972.
[26] J.S. Hadamard, Mouvement permanent lent d'une sphere liquide et visqueuse dans un liquide visqueux, C. R. Acad. Sci. 152 (1911) 1735.
[27] R.M. Davies, Sir G.I. Taylor, The mechanics of large bubbles rising through extended liquids and through liquids in tubes, Proc. Roy. Soc. London Ser. A. 200 (1950) 375–390.
[28] M. Ishii, T.C. Chawla, Local drag laws in dispersed two-phase flow, ANL-79-105, 1979.
[29] G.B. Wallis, The terminal speed of single drops or bubbles in an infinite medium, Internat. J. Multiph. Flow 1 (1974) 491–511.
[30] A. Tomiyama, G.P. Celata, S. Hosokawa, S. Yoshida, Terminal velocity of single bubbles in surface tension force dominant regime, in: 39th European Two-Phase Flow Group Meeting, Aveiro, Portugal, 18–20 June, 2001, Paper F-2, pp. 1–8.
[31] P. Di Marco, W. Grassi, Motivation and results of a long-term research on pool boiling heat transfer in low gravity, keynote lecture, in: G.P. Celata, P. Di Marco, A. Goulas, A. Mariani (Eds.), Experimental Heat Transfer, Fluid Mechanics and Thermodynamics, 2001, pp. 35–53.
[32] P. Di Marco, W. Grassi, S. Hosokawa, G. Memoli, T. Takamasa, A. Tomiyama, Influence of electric field on single gas-bubble growth and detachment in microgravity, in: 39th European Two-Phase Flow Group Meeting, Aveiro, Portugal, 18–20 June, 2001, Paper F-4, pp. 1–9.
[33] M. Danti, P. Di Marco, W. Grassi, G. Memoli, Effect of an external electric field on bubble dynamics: Preliminary study, in: Proc. XVIII UIT National Conference, Cernobbio, June 28–30, 2000, pp. 715–728.
[34] Fluoroinert Liquids Handbook, 3M, pp. 1–56.
[35] R.M. Wellek, A.K. Agrawal, A.H.P. Skelland, AIChE J. 12 (1966) 854–862.
[36] Sir H. Lamb, Hydrodynamics, 6th Edition, Dover, New York, 1932, Art. 275. Chapter 9.
[37] A. Prosperetti, Free oscillations of drops and bubbles: The initial value problem, J. Fluid Mech. 100 (1980) 333–347.
[38] C.A. Miller, L.E. Scriven, The oscillations of a fluid droplet immersed in another fluid, J. Fluid Mech. 32 (1968) 417–435.
[39] R.M. Edge, C.D. Grant, The terminal velocity and frequency of oscillation of drops in pure systems, Chem. Engrg. Sci. 26 (1971) 1001–1012.
[40] R.R. Schroeder, R.C. Kintner, Oscillations of drops falling in a liquid field, AIChE J. 11 (1965) 1–8.